PAPER

Check for updates

Supramolecular assembly of isomeric SN-38 prodrugs regulated by conjugation sites†

Zhenhai Tang, Jianhua Zhang, Wenting Li, Kaiying Wen, Zhipeng Gu, [ID] Dongdong Zhou [ID] * and Hao Su [ID] *

Supramolecular polymers (SPs) are an emerging class of drug transporters employed to improve drug therapy. Through the rational design of self-assembling monomers, one can optimize the properties of the resulting supramolecular nanostructures, such as size, shape, surface chemistry, release, and, therefore, biological fates. This study highlights the design of isomeric SN38 prodrugs through the conjugation of hydrophilic oligo(ethylene glycol) (OEG) with hydroxyls at positions 10 and 20 on hydrophobic SN-38. Self-assembling prodrug (SAPD) isomers 10-OEG-SN38 and 20-OEG-SN38 can self-assemble into giant nanotubes and filamentous assemblies, respectively, *via* aromatic associations that dominate self-assembly. Our study reveales the influence of modification sites on the assembly behavior and ability of the SN38 SAPDs, as well as drug release and subsequent *in vitro* and *in vivo* antitumor effects. The SAPD modified at position 20 exhibits stronger $\pi-\pi$ interactions among SN38 units, leading to more compact packing and enhanced assembly capability, whereas OEG at position 10 poses steric hindrance for aromatic associations. Importantly, owing to its higher chemical and supramolecular stability, 20-OEG-SN38 outperforms 10-OEG-SN38 and irinotecan, a clinically used prodrug of SN38, in a CT26 tumor model, demonstrating enhanced tumor growth inhibition and prolonged animal survival. This study presents a new strategy of using interactions among drug molecules as dominating features to create supramolecular assemblies. It also brings some insights into creating effective supramolecular drug assemblies *via* the engineering of self-assembling building blocks, which could contribute to the optimization of design principles for supramolecular drug delivery systems.

Introduction

Supramolecular polymers (SPs) constructed *via* the non-covalent linkage of monomeric units offer great advantages in improving the delivery of drugs.[1–3] One unique feature is that the physiochemical properties of supramolecular nanostructures can be facilely controlled *via* the molecular-level design of self-assembling building blocks. For example, the morphologies of peptide assemblies are highly sequence-specific[4–6] and sensitive to the amino acid position in isomeric peptide sequences.[7–9] In other examples, the self-assembly behavior of monomeric building blocks is controlled by the attachment and removal of enzyme cleavable pendant functional groups, enabling the sol–gel transition of supramolecular materials.[10,11] In addition, the composition and functionality of SPs can be tuned *via* the supramolecular copolymerization of

multiple monomers.[12,13] Among these monomeric units, self-assembling prodrugs (SAPDs) have been recently recognized as a class of novel monomers of particular interest that are capable of spontaneously associating into SPs in aqueous solutions, achieving self-formulation and self-delivery of active drugs.[14,15] Conjugation of hydrophobic drugs to hydrophilic auxiliaries affords amphiphilic prodrugs, which subsequently self-assemble into discrete drug nanostructures in aqueous environments. Compared with traditional nanomedicines prepared *via* drug encapsulation, this strategy avoids external carriers, which could potentially overcome the heterogeneity between drug molecules and carriers, thereby significantly increasing drug loading and reducing the toxicity risk from drug leakage and external carrier materials. The physicochemical properties, such as size, shape, surface chemistry, internal ordering, and stability, of the resulting drug assemblies can be meticulously regulated through the design and refinement of the prodrug molecular structure, thereby offering high levels of operability.[16,17] For example, block copolymer-drug conjugates consisting of poly(ethylene glycol)-poly(α,β-aspartic acid) (PEG-*b*-PAsp) and doxorubicin can assemble into drug-containing micelles.[18] The Chikoti group synthesized a class of chimeric

College of Polymer Science and Engineering, State Key Laboratory of Polymer Materials Engineering, Sichuan University, Chengdu 610065, China.
E-mail: hsu@scu.edu.cn, zhoudd@scu.edu.cn

† Electronic supplementary information (ESI) available. See DOI: https://doi.org/10.1039/d4tb00717d

polypeptide–drug conjugates that can self-assemble into sub-100-nm-sized nanoparticles.[19] The modification of small molecule drugs with short peptides created a library of peptide–drug conjugates that enable the formation of filamentous assemblies in aqueous solutions.[20,21]

Irinotecan (CPT-11), a derivative of the prototypical anti-cancer drug camptothecin (CPT), manifests cytotoxicity by arresting the DNA replication process through the entrapment of topoisomerase I and remains a prevalent treatment modality for advanced colorectal cancer in the clinic.[22–24] Nonetheless, the metabolic conversion rate of CPT-11 is low and highly depends on the esterase level in the patients, causing drawbacks such as rapid clearance from the bloodstream and nonspecific cytotoxicity.[25] Studies have indicated that the irinotecan needs to hydrolyze to the parent drug SN-38 to exert its therapeutic efficacy, and the *in vitro* cytotoxicity of the parent drug, SN38, is 100–1000 times greater than that of CPT-11.[26] Structurally, SN38 incorporates an additional hydroxyl compared to CPT; however, similar to CPT, it suffers from exceedingly poor solubility in water, ranging from 2 to 5 μg ml^{-1}, instability at physiological pH, and strong binding with plasma proteins, which hinders its direct use in the clinic.[27] Despite these problems, the strong potency of SN-38 attracts great interest in making it a great candidate for more effective cancer treatment.[28,29] Considering the molecular structure of SN-38, the inherent strong hydrophobicity of the SN-38 molecules could serve as the driving force in self-assembly, and the π–π stacking interaction among the aromatics could provide directional forces to aggregate one-dimensionally. Therefore, chemical modification to make SN-38 amphiphilic is feasible for creating SAPDs that can self-assemble into supramolecular nanostructures. Simultaneously, the two hydroxyl modification sites on the SN38 molecule afford more possibilities and

Hao Su received his bachelor's degree in polymer science and engineering from Sichuan University in 2013, a master's degree in polymer science from the University of Akron in 2014 under the supervision of Prof Stephen Z. D. Cheng, and PhD in chemical and biomolecular engineering from the Johns Hopkins University in 2019 under the supervision of Prof. Honggang Cui. He was Post-doctoral Fellow with Prof. Bert Meijer at the Institute for Complex Molecular Systems at the Eindhoven University of Technology from 2019 to 2021. He is currently Assistant Professor in the Department of Polymer Science and Engineering at Sichuan University. He is a member of the Early Career Board of Biomacromolecules. His research interests include the design, synthesis and self-assembly of prodrugs, peptides and polypeptides for applications in drug delivery and tissue engineering.

Hao Su

flexibility in the amphiphilic prodrug design.[30] For example, the Cui group synthesized a nonionic self-assembling prodrug hydrogelator (SAPHs) by conjugating SN38 on the 20-site with a peptide auxiliary decorated with hydrophilic oligo(ethylene glycol) (OEG) on the lysine side chain.[31] Remarkably, this prodrug molecule spontaneously assembles into stable nanofibers in water and, interestingly, under physiological conditions, which can respond to the Hofmeister effect to transition into a gel, thereby enabling the sustained release of SN38. Yang and colleagues synthesized a negatively charged prodrug, HCPT (10-site)-peptide (FFERGD), and co-assembled it with cisplatin.[32] The resultant dual-drug assembly, aided by the positive charge of cisplatin on its outer surface, efficiently penetrates the cell nucleus, achieving promising therapeutic outcomes both *in vitro* and *in vivo*. Li, Zhang and colleagues conjugated SN38 with RGDR and HKD peptides through β-sheet peptide sequences to form co-assembled nanofibers. These fibrous nano-prodrugs effectively suppressed primary tumors and lung metastasis by upregulating integrin expression, providing a synergistic approach to chemotherapy and immunotherapy.[33] To create SN-38 filamentous assemblies, current strategies predominantly involve the use of peptides as the hydrophilic auxiliaries, which could provide hydrogen bonding interactions to enhance the self-assembly capability.[17,34] However, in some cases, the hydrogen bonding and π–π associations could also compete with each other, reducing the orderliness of molecular arrangements.[35] Considering that the supramolecular self-assembly could occur in a π–π association-controlled manner, the utilization of peptide segments as structural domains is unnecessary. Therefore, we envision that solely using the interactions from SN-38 could also direct ordered molecular arrangements. The conjugation of short hydrophilic segments could simplify the molecular design, in which SN38 plays both therapeutic and structural roles. In addition, because SN38 has two conjugation sites, self-assembly behavior could be affected by modifying different hydroxyl positions.

In this study, we directly modify the 10- and 20-site hydroxyl groups of SN38 with pentaethylene glycol monomethyl ether (OEG$_5$-OH) by carbonate bond, giving two prodrugs (10-OEG-SN38 and 20-OEG-SN38) that exist as isomers. The use of OEG as hydrophilic segments does not introduce extra intermolecular interactions to ensure the dominant role of π–π associations; simultaneously, it also provides neutral surface chemistry and steric effect, which could potentially reduce protein absorption and improve pharmacokinetics in circulation. The incorporation of the carbonate bond enables the degradation of the prodrugs through either chemical or enzymatic hydrolysis to release the parent drug SN-38. Luckily, both SN-38 prodrugs can self-assemble into one-dimensional nanostructures in aqueous solutions. This straightforward molecular design also enables a more intuitive understanding of how different modification sites influence the assembly behavior and capability of SN38. The findings of our study indicate a strong correlation between the π–π interactions among SN38 molecules and the sites of modification. Specifically, when the hydroxyl group at position 20 is modified, it tends to form filamentous structures with a regular chiral arrangement.

This journal is © The Royal Society of Chemistry 2024

J. Mater. Chem. B, 2024, **12**, 6146–6154 | **6147**

This tendency leads to more compact packing and enhanced assembly capabilities. Conversely, the chiral stacking of SN38 is disrupted when modification occurs at the 10-site, resulting in compromised assembly capacity. These disparities directly affect the drug release, cytotoxicity and therapeutic efficacy of the SAPDs both *in vitro* and *in vivo*. Our results provide an example of using interactions among drug molecules as dominating features to create supramolecular assemblies and the strategic selection of the most appropriate hydroxyl modification sites for designing SN38 SAPD to maximize its performance in self-assembly and therapy.

Experimental section

1 Synthesis of OEG-NO$_2$

Pentaethylene glycol monomethyl ether (OEG$_5$-OH, 1.00 g, 3.9 mmol), 4-dimethylamino pyridine (DMAP, 1.65 g, 13.5 mmol) and 4-nitrobenzoyl chloride were mixed together into dry DCM (30 ml) and then stirred at room temperature overnight. The reaction mixture was evaporated to remove the solvent, and the residue was further purified by chromatography on silica gel with EA/PE (1/9 to 1/1) and then EA/MeOH (19/1) as the eluent to obtain the OEG-NO$_2$ (colorless oil, 1.2 g, 73%). ^{1}H NMR (300 MHz; CDCl3; ppm): δ 3.38 (s, 3H), 3.50–3.85 (m, 18H), 4.40–4.47 (m, 2H), 7.34–7.46 (m, 2H), 8.22–8.34 (m, 2H). MS (ESI-MS) *m/z*: [M + H]$^+$ calculated for C$_{18}$H$_{27}$NO$_{10}$, 418.16; found, 418.05.

2 Synthesis of 10-OEG-SN38

SN38 (0.34 g, 0.86 mmol) was suspended in a DCM solution (20 ml) of OEG-NO$_2$ (0.3 g, 0.72 mmol) and triethylamine (0.36 g, 3.59 mmol). The reaction mixture was stirred for 24 hours. After removing the solvent under a vacuum, the residue was first purified by flash chromatography on silica gel with DCM/MeOH (10/1) and then by RP-HPLC (10-SN38-OEG, white solid, 0.3 g, 62%). ^{1}H NMR (300 MHz; CDCl$_3$; ppm): δ 1.0–1.08 (t, 3H), 1.36–1.44 (s, 3H), 1.81–1.98 (m, 2H), 3.10–3.22 (q, 2H), 3.34–3.41 (s, 3H), 3.49–3.91 (m, 20H), 4.44–4.51 (m, 2H), 5.22–5.36 (m, 3H), 5.71–5.80 (d, 1H), 7.61–7.70 (t, 2H), 7.90–7.96 (s, 1H), 8.21–8.29 (d, 1H). MS (ESI-MS) *m/z*: [M + H]$^+$ calculated for C$_{34}$H$_{42}$N$_2$O$_{12}$, 670.27; found, 671.12.

3 Synthesis of 20-OEG-SN38

SN38 (1 g, 2.55 mmol) was suspended in a solution of di-*tert*-butyl dicarbonate (0.72 g, 3.3 mmol) and triethylamine (0.52 g, 5 mmol) in DCM (40 ml). After being stirred at room temperature for 48 h, the resulting mixture was washed three times with 0.5 M HCl (40 ml) and brine (40 ml) and then dried using anhydrous sodium sulfate to obtain 10-BOC-SN38 (pale-yellow solid, 1.02 g, 92%). ^{1}H NMR (300 MHz; CDCl$_3$; ppm): δ 0.97–1.10 (t, 3H), 1.34–1.46 (s, 3H), 1.52–1.68 (s 9H), 1.81–1.99 (m, 2H), 3.08–3.24 (q, 2H), 5.21–5.37 (m, 3H), 5.68–5.82 (d, 1H), 7.59–7.72 (t, 2H), 7.85–7.94 (s, 1H), 8.19–8.27 (d, 1H).

10-BOC-SN38 (0.4 g, 0.9 mmol), OEG-NO$_2$ (0.46 g, 1 mmol) and DMAP (0.25 g, 2 mmol) were dissolved in DCM (30 ml). The reaction mixture was heated reflux at 55 °C and stirred

overnight. The yellow solution was concentrated *in vacuo*, and the residue was further purified using RP-HPLC. The product fractions were combined and lyophilized to give 10-Boc-20-OEG-SN38 (pale-yellow solid, 0.3 g, 43%). ^{1}H NMR (300 MHz; CDCl$_3$; ppm): δ 0.95–1.04 (t, 3H), 1.35–1.43 (s, 3H), 1.61–1.64 (s, 9H), 2.08–2.34 (m, 2H), 3.12–3.21 (q, 2H), 3.35–3.40 (s, 3H), 3.5–3.75 (m, 17H), 4.19–4.32 (m, 2H), 5.22–5.30 (s, 2H), 5.35–5.74 (q, 2H) 7.28–7.33 (s, 1H), 7.64–7.72 (d 1H), 7.88–7.93 (s, 1H), 8.20–8.26 (d, 1H).

Trifluoroacetic acid (TFA, 0.88 g, 7.8 mmol) was added dropwise to a solution of 10-BOC-20-OEG-SN38 (0.3 g, 0.39 mmol) in DCM (10 ml). The resulting mixture was washed with a saturated solution of NaHCO$_3$ and dried over anhydrous sodium sulfate. The mixture was concentrated *in vacuo* to obtain the 20-OEG-SN38 (bright yellow powder, 0.22 g, 84.6%). ^{1}H NMR (300 MHz; CDCl$_3$; ppm): δ 1.01–1.05 (t, 3H), 1.25–1.38 (s, 3H), 2.10–2.30 (m, 2H), 2.96–3.10 (q, 2H), 3.35–3.45 (s, 3H), 3.46–3.78 (m, 19H), 4.13–4.33 (m, 2H), 5.02–5.18 (s, 2H), 5.32–5.77 (q, 2H) 7.28–7.30 (s, 1H), 7.31–7.38 (s 1H), 7.44–7.55 (d, 1H), 8.01–8.12 (d, 1H). MS (ESI-MS) *m/z*: [M + H]$^+$ calculated for C$_{34}$H$_{42}$N$_2$O$_{12}$, 670.27; found, 671.13.

4 Synthesis of di-OEG-SN38

SN38 (0.5 g, 1.274 mmol) was suspended in the solution of triphosgene (0.2647 g, 0.892 mmol) in dry DCM (50 ml). DMAP (0.7165 g, 5.86 mmol) was dissolved in dry DCM (20 ml) and added dropwise to the mixture. After one hour, OEG (0.7073 g, 2.80 mmol) was then added to the mixture and stirred overnight. The mixture was washed with 0.5 M HCl (50 ml × 3) and brine (50 ml × 3). Then, the extracts were dried with anhydrous sodium sulfate. The reaction mixture was concentrated under a vacuum, and the residue was purified using RP-HPLC. The product fractions were combined and lyophilized to produce di-OEG-SN38 (pale-yellow solid, 0.6 g, 50%). ^{1}H NMR (300 MHz; CDCl$_3$; ppm): δ 0.99–1.05 (t, 3H), 1.25–1.39 (s, 3H), 2.10–2.30 (m, 2H), 2.96–3.10 (q, 2H), 3.08–3.78 (m, 46H), 4.17–4.32 (m, 2H), 4.44–4.51 (m, 2H), 5.26 (d, 2H), 5.39–5.69 (q, 2H), 7.30 (s, 1H), 7.67 (dd 1H), 7.94 (d, 1H), 8.24 (d, 1H). [M + H]$^+$ calculated for C$_{46}$H$_{64}$N$_2$O$_{19}$, 948.41; found, 949.13.

Results and discussions

Synthesis of self-assembling SN38 prodrugs

Fig. 1A and Scheme S1 (ESI†) show the molecular design of the studied self-assembling prodrugs (SAPDs), consisting of the hydrophobic SN38 and hydrophilic OEG$_5$-OH. The commercially available SN38 possesses two different hydroxyl groups located at positions 10 and 20, exhibiting varied reactivity when coupled with OEG$_5$-OH *via* carbonate bonds. By carefully regulating the molar ratio between SN38 and OEG$_5$-OH, only phenolic (C10) or both hydroxyl groups were conjugated, yielding mono- and di-functional SN38 (labeled as 10-OEG-SN38 and di-OEG-SN38), respectively. Furthermore, the phenolic hydroxyl group could be protected by *tert*-butyloxycarbonyl (Boc), and the residual C20-hydroxyl group was then capped by OEG$_5$-OH.

6148 | *J. Mater. Chem. B*, 2024, **12**, 6146–6154

This journal is © The Royal Society of Chemistry 2024

Fig. 1 Schematic illustration of the design and synthesis of SN38 SAPDs (A). Comparison of the RP-HPLC chromatograms of 10-OEG-SN38 and 20-OEG-SN38 (B) and comparison of ^{1}H NMR spectra of 10-OEG-SN38 and 20-OEG-SN38 (C).

Another mono-substituted prodrug (20-OEG-SN38) was obtained after deprotecting and served as the regio-isomer of 10-OEG-SN38. Details of the synthesis of these self-assembling prodrugs can be found in Section 1–4 and Fig. S1–S6 (ESI†).

The HPLC trace of each compound, as shown in Fig. 1B, displays a narrow and unimodal peak, confirming the high purity of the obtained molecules. The chemical accuracy of each sample was further confirmed by LC-MS, with a series of single m/z peaks in excellent accordance with the calculated values (Fig. S1–S6, ESI†). All these characterizations clearly demonstrate the successful synthesis of the prodrugs. The resultant prodrugs were purified using reversed-phase high-performance liquid chromatography (RP-HPLC), and their chemical structures and purity were fully characterized by nuclear magnetic resonance (NMR), analytical HPLC and liquid chromatography-mass spectrometry (LC-MS). The characteristic resonances of both precursory motifs (SN38 and OEG) could

be captured, and the integration agrees well with the proposed chemical structures.

Interestingly, the subtle variations between samples 10-OEG-SN38 and 20-OEG-SN38, a pair of regio-isomers with the same composition but different architectures, can be clearly identified by HPLC and ^{1}H NMR. The eluting time of sample 20-OEG-SN38 is substantially longer than that of 10-OEG-SN38, which can be well resolved due to the appreciable difference (Fig. 1B). This may indicate that sample 20-OEG-SN38 possesses a stronger hydrophobic interaction. As depicted in Fig. 1C, obvious disparities emerge within the 4–8 ppm range corresponding to various modifications at distinct positions of SN38. Specifically, the 20-OEG-SN38 spectrum exhibits noteworthy variations. The peaks corresponding to OEG proximal to carbonate bonds undergo fragmentation into multiple peaks, accompanied by chemical shift variations from 4.5 ppm to 4.2 ppm due to the influence of the chiral carbon. In contrast, both 10-OEG-SN38

and OEG-NO$_2$ (Fig. 1C and Fig. S1 (ESI†)) exhibit conventional doublet splitting at the same position. Another obvious transformation manifests within the 6–8 ppm regime, indicating the modifications at the 10-site hydroxyl moiety. Evidently, both 10-OEG-SN38 and 10-Boc-SN38 (Fig. 1C and Fig. S3, ESI†) show similar peaks within the 6–8 ppm range, conspicuously distinguishing them from 20-OEG-SN38.

Self-assembly of SN38 prodrugs

After dissolving these samples in an aqueous solution at a concentration of 1 mM and aging overnight at room temperature, transmission electron microscopy (TEM) was utilized to investigate their morphologies. With the alternation of the regio architecture and the number of OEG, different supramolecular nanostructures were observed. 10-OEG-SN38 self-assembled into a unique giant nanotube with 1.842 ± 0.985 μm ($n > 20$) in length and an approximate 64.3 ± 8.9 nm ($n > 50$) in diameter (Fig. 2A and Fig. S7, ESI†). The wall thickness approximates twice the extended length of molecule 10-OEG-SN38 (Fig. S8A, ESI†), indicating that the packing follows a bilayer packing model. The 20-OEG-SN38 assembled into ordered nanofibers with ca. 9.0 ± 1.1 nm ($n > 50$) in diameter and several micrometers in length (Fig. 2C and Fig. S9, ESI†). The varying morphologies reveal the critical importance of regio architecture on the self-assembly behaviors. Moreover, the molecular packing in supramolecular filaments generally follows the core–shell cylindrical fashion, and the diameter is close to the double size as the motif extended length.[36,37] The size of the 20-OEG-SN38 assembly in diameter, however, is more than twice the molecular extended length (Fig. S8B, ESI†), indicating looser molecular packing. With an increased number of OEG, no ordered

structures were observed for di-OEG-SN38, indicating that the increasing hydrophilic region may impede molecular aggregation. For convenience, this sample, which cannot form an ordered nanostructure, is not discussed further.

To further illustrate the molecular arrangement of the regioisomeric prodrugs in the assemblies, we next performed circular dichroism (CD) spectroscopy measurements. 20-OEG-SN38 exhibits two CD negative signals centered at 366 nm and a strong positive signal at 389 nm (Fig. 2D). This type of peak position has been reported in previous studies,[38] resulting from exciton coupling between two adjacent chromophores in a chiral orientation, which indicates a strong exciton coupling between SN38 units. The positive peak at 389 nm suggests a chiral and right-handed helical arrangement of the SN38 molecules within the nanofibers. The CD spectrum of 10-OEG-SN38 shows only a mainly sharp peak at 240 nm (Fig. 2B), which could be attributed to chromophore interactions (n–π*). Nevertheless, there is no 389 nm positive peak in the CD signal, indicating that the modification by OEG at the 10-position disrupts the ordered aromatic packing and chiral orientation of SN38 in the assembly as the hydroxyl is on the aromatic ring. The hydroxyl at the 20-site is far from the aromatic region; therefore, the modification does not disturb the π–π stacking. The results of the CD analysis suggest that various modifications of SN38 at different sites can result in distinct interactions between SN38 SAPDs. Specifically, for 20-OEG-SN38, the regular chiral stacking and closer molecular arrangement may potentially reduce the relative volume of the hydrophobic domain, leading to the formation of core–shell structured nanofibers, while the 10-OEG-SN38 without the chiral stacking feature tends to form a giant nanotube with a bilayer structure.

Self-assembly capability and stability

To investigate the self-assembly capability of these prodrugs, their critical micelle concentrations (CMCs) were determined using dynamic light scattering (DLS). The count rate values of the aqueous solutions at various concentrations were recorded, which underwent a transition accompanying the formation of molecular aggregates. The CMC values of these prodrugs were assessed by plotting the count rate value against the concentration of the sample.[17] As shown in Fig. 3A and B, the mutations were identified when the concentrations were above the CMCs. The critical values are ca. 764 μM for 10-OEG-SN38 and ca. 13 μM for 20-OEG-SN38. It is also noteworthy that the CMC value sometimes differs from the critical assembly concentration (CAC) value. The CAC, above which the molecules start to form well-defined structures, is another key parameter associated with the dynamic feature and stability of supramolecular assemblies.[35] To further illustrate the self-assembly capability of the prodrugs, the CD measurements of 10-OEG-SN38 and 20-OEG-SN38 at different concentrations were carried out. As illustrated in Fig. 3C and D, characteristic peaks inherited from the equilibrium assemblies appear as the solution concentration exceeds the CACs. For example, the distinctive peaks associated with 20-OEG-SN38 at 389 nm disappeared below 20 μM, suggesting the disassembly of

Fig. 2 Supramolecular polymers formed by SAPDs in water. TEM images of supramolecular assemblies of 10-OEG-SN38 (A) and 20-OEG-SN38 (C) at a concentration of 1 mM. CD of 10-OEG-SN38 (1 mM) (B) and 20-OEG-SN38 (200 μM). (D).

6150 | J. Mater. Chem. B, 2024, 12, 6146–6154

This journal is © The Royal Society of Chemistry 2024

Fig. 3 Determination of self-assembly capacity and supramolecular stability. CMC was measured using DLS methods through the mutation of the count rate. 10-OEG-SN38 (A) and 20-OEG-SN38 (B). CD for various concentrations around CAC: 10-OEG-SN38 (C) and 20-OEG-SN38 (D).

nanofibers (Fig. 3C). Meanwhile, concentrations surpassing 900 μM yielded a notable positive peak at 240 nm, indicative of assembly formation for 10-OEG-SN38 (Fig. 3D). The estimated values are 900–1000 μM for 10-OEG-SN38 and 10–20 μM for 20-OEG- SN38. Both CMC and CAC values suggest that the self-assembly capability of 10-OEG-SN38 significantly decreases compared with that of 20-OEG-SN38, which may be due to the reduction of aromatic interactions resulting from the steric hindrance by the attached OEG on the benzene ring. These results indicate that various modification sites of SN38 significantly affect their associations and molecular arrangement, further affecting the assembly capability.
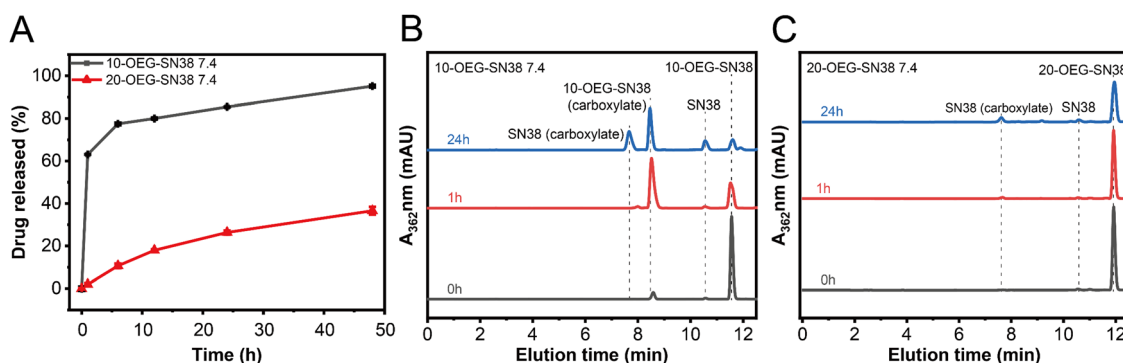
Drug release

To explore drug release properties, we performed degradation experiments at 37 °C in PBS solutions with a concentration of 200 μM. Because the solubility of SN38 is extremely poor, we chose to utilize the remaining ratio of SAPDs for detection by RP-HPLC. As shown in Fig. 4A, 20-OEG-SN38 exhibits a lower

degradation rate than that of 10-OEG-SN38, indicating a higher level of stability. Fig. 4B and C show a significant difference in the stability and degradation profiles between isomers at pH 7.4 monitored *via* analytical HPLC. Two peaks were observed in HPLC traces in the first hour, located at 8.5 min and 12 min, with the remaining ratio of 10-OEG-SN38 rapidly weakening to 40% (Fig. 4B). Monitored by LC-MS, the additional peak at 8.5 min was assigned to the carboxylate form of the prodrug (Scheme S2, ESI†) rather than the parent drug SN38 after carbonate cleavage. To confirm the pH-dependent hydrolysis of lactone, we investigated the stability of lactone in SN38 at pH 5.4. The corresponding peak is absent, revealing that the lactone stability of 10-OEG-SN38 is promoted at a lower pH value (Fig. S10, ESI†). Conversely, in the case of 20-OEG-SN38, the carboxylate form was not captured at both pH levels, which may be attributed to the enhanced stability of lactone by chemical modification at the 20-site.[39] It is well known that the release of the SN38 parent drug incorporates the disassembly of supramolecular structures and the subsequent hydrolysis of carbonate bonds. Here, benefiting from the lower CMC, 20-OEG-SN38 maintains a stable assembly status at a concentration of 200 μM, which can reduce solvent and ion contact and increase the stability of prodrugs. Our results reveal that the regio architecture can significantly influence the drug release process by altering chemical stability and self-assembly capability.

Cytotoxicity

We next studied the *in vitro* cytotoxicity against colorectal cancer cells CT26 and breast cancer cells MDA-MB-231 using SAPDs and the controls (*i.e.*, the parent drug SN38 and clinically used prodrug irinotecan) at various concentrations. The SAPDs were incubated with tumor cells for 48 hours, and their efficacy was evaluated by applying MTT methods *via* a dose–response relationship assay based on SN38 concentration (Fig. 5). Fig. 5A illustrates that the IC$_{50}$ values of irinotecan, a clinical medication used for colorectal cancer, reach approximately 74 443 nM for CT26 cancer cells. Both SN38 SAPDs exhibit lower IC$_{50}$ values with 518 nM for the 10-site and 1517 nM for the 20-site, suggesting a more effective inhibition of colorectal tumor cells in comparison to irinotecan. In contrast

Fig. 4 Drug release of SN38 SAPDs at 200 μM in PBS at pH 7.4. Drug release plots of SAPDs (A) and comparison of HPLC spectra at different time points at pH 7.4:10-OEG-SN38 (B) and 20-OEG-SN38 (C).

This journal is © The Royal Society of Chemistry 2024

J. Mater. Chem. B, 2024, **12**, 6146–6154 | **6151**

Fig. 5 *In vitro* cell cytotoxicity of 10/20-OEG-SN38 against CT-26 colorectal cancer cells (A) and MDA-MB-231 breast cancer cells (B), with both free SN38 and irinotecan as controls (48-h incubation).

to CT26 cells, both SAPDs exhibit a higher IC_{50} in MDA-MB-231 cells. This lower toxicity may arise from the reduction of the degradation rate of carbonate bonds due to the relatively lower pH value within the microenvironment of breast cancer cells in comparison to colorectal cancer cells.[40] It is noteworthy that the efficacies of SAPDs are just slightly lower than those of the parent drug SN38, indicating that both SAPDs can effectively release the parent drug in the cellular environment. Moreover, there are still differences in efficacy between the isomers depending on their concentration levels.

At lower concentrations, 10-OEG-SN38 shows a higher level of cytotoxicity due to the faster hydrolysis of the carbonate bond with the phenolic hydroxyl group. Nevertheless, at concentrations ranging from 50 to 100 µM, 20-OEG-SN38 exhibits a lower cell survival rate and shows a continuous decreasing trend, especially in MDA-MB-231 cells (Fig. 5B). As mentioned above, the lactone ring of SN38 was easily opened to reduce toxicity when modified on the 10-site but remained stable on the 20-site. As the concentration increases, 20-site may release more active ingredients compared to 10-site at the same concentration, resulting in a variety of toxicity between isomers. Moreover, above its CMC (13 µM), the self-assembled nanostructures may play a certain role in cell internalization. Therefore, we can conclude that both SAPDs have excellent *in vitro* cytotoxicity, underscoring their substantial anticancer potential.

In vivo antitumor efficacy

To further understand how the regio architecture of SAPDs affects their *in vivo* performance, the antitumor efficacies of the regio-isomeric prodrugs were evaluated in a CT26 tumor model of BALB/c mice (see details in ESI†). The irinotecan dosage was set at 30 mg kg^{-1} every two days near its maximum tolerated dosage.[41] Similarly, the dosage of SN38 in our prodrugs was 34.3 mg kg^{-1}, matching the SN38 equivalent in irinotecan. When the tumor volume reached ∼100 mm^3 after tumor inoculation, the drugs were administered once every two days for six doses (*i.e.*, day 1, 3, 5, 7, 9, and 11) using physiological saline as a blank control. During the experiment, the weight and tumor volume of the mice were recorded as detection indicators of efficacy and safety. The body weights and tumor volumes of the mice are shown in Fig. 6A and B. After the fifth dose (day 9), the tumor volumes of the saline, irinotecan, 10-OEG-SN38, and 20-OEG-SN38 groups approached 586 mm^3, 410 mm^3, 124 mm^3, and 98 mm^3, respectively. Both SAPDs exhibited a more significant inhibitory effect on tumor growth compared with irinotecan, probably attributed to higher cytotoxicity and improved pharmacokinetics. Interestingly, although the group receiving 10-OEG-SN38 showed significant inhibition of tumor growth, we observed severe weight loss and even death in the studied animals within 11 days (Fig. 6A and C). This observation suggests that the 10-OEG-SN38 has severe toxicities in the animals studied. With a high CMC, 10-OEG-SN38 is rapidly diluted to small molecules in the bloodstream after injection, possibly leading to a fast drug release and causing toxicity to normal tissues. However, throughout the 20-OEG-SN38 treatment period, the average weight of the mice remained stable (Fig. 6A) and the 20-OEG-SN38 group showed the slowest tumor volume growth among all the treated groups (Fig. 6B). Additionally, the administration of 20-OEG-SN38 increased the median survival from 15 d (the control group) to 23 d, while the median survivals of the other groups were 11 d (10-OEG-SN38) and 17 d (irinotecan) (Fig. 6C). A reasonable explanation is that 20-OEG-SN38 can retain its nanostructure with low CMC (13 µM) upon dilution in the circulation. This could prevent rapid renal clearance and prolong circulation to improve efficacy and safety. Our results revealed the differences in toxicity and efficacy of SN38 SAPDs when modified

Fig. 6 *In vivo* antitumor efficacy of SAPDs using irinotecan and saline as the control group with 8 mice in each group. Relative body weight (A), tumor volume (B), and percent survival (C) plots of mice between isomers.

at 10-site and 20-site, establishing the correlations among molecular design, supramolecular stability, *in vitro* cytotoxicity and *in vivo* efficacy.

Conclusions

In this article, we synthesized a group of isomers *via* modification at different hydroxyl sites on SN38 to investigate their self-assembly behavior and biological functions. The SN38 SAPDs were self-assembled into giant nanotubes and nanofibers when OEG was anchored onto 10- or 20-positions. The SN38 SAPD with OEG at position 10 showed weaker aromatic associations and lower assembly capacity compared with SN-38 modified at position 20 due to the steric hindrance from OEG on the benzene ring that disrupted the close π–π stacking. The chemical and supramolecular stability of SAPDs can further influence the drug release, cytotoxicity, and therapeutic efficacy of the SAPDs both *in vitro* and *in vivo*. 20-OEG-SN38 exhibited lower cytotoxicity because of the slower hydrolysis of its carbonate bond; however, its therapeutic efficacy in tumor inhibition was better than that of commercial irinotecan. The 20-OEG-SN38 with a lower CMC retains its supramolecular integrity in the circulation, resulting in longer circulation and significantly retarding the growth of the tumor. Overall, our results indicate that the isomerization of SN38-OEG had significant effects on their associations, molecular arrangement in the assemblies, assembly capability, and, eventually, anticancer effects. Our work also presented a simplified design of amphiphilic prodrugs *via* direct OEGylation and gave an example of solely using the molecular interactions among drug units to create supramolecular drug assemblies without other directional intermolecular forces, such as hydrogen bonding. We hope that the current research can provide new insights into the selective modification of therapeutics into SAPDs and motivate the future design of simple SAPD systems.

Author contributions

Z. T. and H. S. designed research; Z. T., J. Z., W. L., and K. W. performed research; Z. T., D. Z., and H. S. analysed data; Z. G., D. Z., and H. S. supervised the project; Z. T., D. Z., and H. S. wrote and revised the paper.

Conflicts of interest

There are no conflicts to declare.

Acknowledgements

Notes and references

1 H. Acar, S. Srivastava, E. J. Chung, M. R. Schnorenberg, J. C. Barrett, J. L. LaBelle and M. Tirrell, Self-Assembling Peptide-Based Building Blocks in Medical Applications, *Adv. Drug Delivery Rev.*, 2017, **110–111**, 65–79.

2 M. J. Webber, E. A. Appel, E. W. Meijer and R. Langer, Supramolecular Biomaterials, *Nat. Mater.*, 2016, **15**(1), 13–26.

3 T. Aida, E. W. Meijer and S. I. Stupp, Functional Supramolecular Polymers, *Science*, 2012, **335**(6070), 813–817.

4 P. W. J. M. Frederix, G. G. Scott, Y. M. Abul-Haija, D. Kalafatovic, C. G. Pappas, N. Javid, N. T. Hunt, R. V. Ulijn and T. Tuttle, Exploring the Sequence Space for (Tri-)Peptide Self-Assembly to Design and Discover New Hydrogels, *Nat. Chem.*, 2015, **7**(1), 30–37.

5 Y. Zhang, T. Zhou, Y. Qi, Y. Li, Y. Zhang, Y. Zhao, H. Han and Y. Wang, Engineered Assemblies from Isomeric Penta-peptides Augment Dry Eye Treatment, *J. Controlled Release*, 2024, **365**, 521–529.

6 Y. Wang, Y. Lyu and Z. Li, Constitutionally Isomeric Peptides: Subtle Changes Leading to Dramatic Differences in Properties, *ACS Appl. Eng. Mater.*, 2024, DOI: **10.1021/acsaenm.3c00787**.

7 H. Cui, A. G. Cheetham, E. T. Pashuck and S. I. Stupp, Amino Acid Sequence in Constitutionally Isomeric Tetrapeptide Amphiphiles Dictates Architecture of One-Dimensional Nano-structures, *J. Am. Chem. Soc.*, 2014, **136**(35), 12461–12468.

8 A. Lampel, S. A. McPhee, H.-A. Park, G. G. Scott, S. Humagain, D. R. Hekstra, B. Yoo, P. W. J. M. Frederix, T.-D. Li, R. R. Abzalimov, S. G. Greenbaum, T. Tuttle, C. Hu, C. J. Bettinger and R. V. Ulijn, Polymeric Peptide Pigments with Sequence-Encoded Properties, *Science*, 2017, **356**(6342), 1064–1068.

9 Y. Wang, K. Kaur, S. J. Scannelli, R. Bitton and J. B. Matson, Self-Assembled Nanostructures Regulate H2S Release from Constitutionally Isomeric Peptides, *J. Am. Chem. Soc.*, 2018, **140**(44), 14945–14951.

10 Z. Liu, J. Guo, Y. Qiao and B. Xu, Enzyme-Instructed Intra-cellular Peptide Assemblies, *Acc. Chem. Res.*, 2023, **56**(21), 3076–3088.

11 M. Yi, Z. Feng, H. He, D. Dinulescu and B. Xu, Evaluating Alkaline Phosphatase-Instructed Self-Assembly of d-Peptides for Selectively Inhibiting Ovarian Cancer Cells, *J. Med. Chem.*, 2023, **66**(14), 10027–10035.

12 S. I. S. Hendrikse, L. Su, T. P. Hogervorst, R. P. M. Lafleur, X. Lou, G. A. van der Marel, J. D. C. Codee and E. W. Meijer, Elucidating the Ordering in Self-Assembled Glycocalyx Mimicking Supramolecular Copolymers in Water, *J. Am. Chem. Soc.*, 2019, **141**(35), 13877–13886.

This journal is © The Royal Society of Chemistry 2024

J. Mater. Chem. B, 2024, **12**, 6146–6154 | **6153**

13 H. Su, W. Zhang, H. Wang, F. Wang and H. Cui, Paclitaxel-Promoted Supramolecular Polymerization of Peptide Conjugates, *J. Am. Chem. Soc.*, 2019, **141**(30), 11997–12004.

14 A. G. Cheetham, R. W. Chakroun, W. Ma and H. Cui, Self-Assembling Prodrugs, *Chem. Soc. Rev.*, 2017, **46**(21), 6638–6663.

15 H. Su, J. M. Koo and H. Cui, One-Component Nano-medicine, *J. Controlled Release*, 2015, **219**, 383–395.

16 H. Ren, X.-Z. Zeng, X.-X. Zhao, D. Hou, H. Yao, M. Yaseen, L. Zhao, W. Xu, H. Wang and L.-L. Li, A Bioactivated in Vivo Assembly Nanotechnology Fabricated NIR Probe for Small Pancreatic Tumor Intraoperative Imaging, *Nat. Commun.*, 2022, **13**(1), 418.

17 C. H. Liang, Y. X. Chen, D. B. Zheng, T. Y. Xu, G. J. Pu, Y. M. Chen, L. Wang, Z. M. Yang and H. M. Wang, Pathway-Dependent Supramolecular Polymerization of Campto-thecin Derivatives into Filaments for Chemotherapy and Imaging. *Appl, Mater. Today*, 2020, **20**, 100787.

18 K. Kataoka, A. Harada and Y. Nagasaki, Block Copolymer Micelles for Drug Delivery: Design, Characterization and Bio-logical Significance, *Adv. Drug Delivery Rev.*, 2012, **64**, 37–48.

19 J. Bhattacharyya, J. J. Bellucci, I. Weitzhandler, J. R. McDaniel, I. Spasojevic, X. Li, C.-C. Lin, J.-T. A. Chi and A. Chilkoti, A Paclitaxel-Loaded Recombinant Polypeptide Nanoparticle Outperforms Abraxane in Multiple Murine Cancer Models, *Nat. Commun.*, 2015, **6**(1), 7939.

20 H. Ren, X.-Z. Zeng, X.-X. Zhao, D. Hou, H. Yao, M. Yaseen, L. Zhao, W. Xu, H. Wang and L.-L. Li, A Bioactivated in Vivo Assembly Nanotechnology Fabricated NIR Probe for Small Pancreatic Tumor Intraoperative Imaging, *Nat. Commun.*, 2022, **13**(1), 418.

21 Y. Fang and H. Wang, Molecular Engineering of Peptide–Drug Conjugates for Therapeutics, *Pharmaceutics*, 2022, **14**(1), 212.

22 Y. Pommier, Topoisomerase I Inhibitors: Camptothecins and Beyond, *Nat. Rev. Cancer*, 2006, **6**(10), 789–802.

23 A. Makimoto, H. Mugishima, T. Taga, Y. Ishida, Y. Nagatoshi, K. Ida, M. Kumagai, T. Kimura, Y. Ohashi and M. Kaneko, Registration-Directed Phase 1/2 Trial of Irinotecan for Pedia-tric Solid Tumors, *Pediatr. Int.*, 2019, **61**(5), 453–458.

24 R. H. J. Mathijssen, R. J. van Alphen, J. Verweij, W. J. Loos, K. Nooter, G. Stoter and A. Sparreboom, Clinical Pharma-cokinetics and Metabolism of Irinotecan (CPT-11), *Clin. Cancer Res.*, 2001, **7**(8), 2182–2194.

25 C. Bailly, Irinotecan: 25 Years of Cancer Treatment, *Phar-macol. Res.*, 2019, **148**, 104398.

26 Y. Huang, L. Wang, Z. Cheng, B. Yang, J. Yu, Y. Chen and W. Lu, SN38-Based Albumin-Binding Prodrug for Efficient Targeted Cancer Chemotherapy, *J. Controlled Release*, 2021, **339**, 297–306.

27 J. Zhao, S. Ma, Y. Xu, X. Si, H. Yao, Z. Huang, Y. Zhang, H. Yu, Z. Tang, W. Song and X. Chen, *In Situ* Activation of STING Pathway with Polymeric SN38 for Cancer Chemoim-munotherapy, *Biomaterials*, 2021, **268**, 120542.

28 Y. Zheng, X. Yan, Y. Wang, X. Duan, X. Wang, C. Chen, D. Tian, Z. Luo, Z. Zhang and Y. Zeng, Hydrophobized SN38 to Redox-Hypersensitive Nanorods for Cancer Therapy, *J. Mater. Chem. B*, 2019, **7**(2), 265–276.

29 Y. Liu, H. Piao, Y. Gao, C. Xu, Y. Tian, L. Wang, J. Liu, B. Tang, M. Zou and G. Cheng, Comparison of Two Self-Assembled Macromolecular Prodrug Micelles with Different Conjugate Positions of SN38 for Enhancing Antitumor Activity, *Int. J. Nanomed.*, 2015, **10**, 2295–2311.

30 X. Yang, H. Lu, Y. Tao, L. Zhou and H. Wang, Spatiotem-poral Control over Chemical Assembly in Living Cells by Integration of Acid-Catalyzed Hydrolysis and Enzymatic Reactions, *Angew. Chem., Int. Ed.*, 2021, **60**(44), 23797–23804.

31 H. Wang, H. Su, T. Xu and H. Cui, Utilizing the Hofmeister Effect to Induce Hydrogelation of Nonionic Supramolecular Polymers into a Therapeutic Depot, *Angew. Chem., Int. Ed.*, 2023, **62**(43), e202306652.

32 Y. Cai, H. Shen, J. Zhan, M. Lin, L. Dai, C. Ren, Y. Shi, J. Liu, J. Gao and Z. Yang, Supramolecular "Trojan Horse" for Nuclear Delivery of Dual Anticancer Drugs, *J. Am. Chem. Soc.*, 2017, **139**(8), 2876–2879.

33 Y. Cai, B. Zhu, X. Shan, L. Zhou, X. Sun, A. Xia, B. Wu, Y. Yu, H. H. Zhu, P. Zhang and Y. Li, Inhibiting Endothelial Cell-Mediated T Lymphocyte Apoptosis with Integrin-Targeting Peptide–Drug Conjugate Filaments for Chemoimmuno-therapy of Triple-Negative Breast Cancer, *Adv. Mater.*, 2024, **36**(3), 2306676.

34 S. Zeng, H. Ou, Z. Gao, J. Zhang, C. Li, Q. Liu and D. Ding, HCPT-Peptide Prodrug with Tumor Microenvironment -Responsive Morphology Transformable Characteristic for Boosted Bladder Tumor Chemotherapy, *J. Controlled Release*, 2021, **330**, 715–725.

35 H. Su, F. Wang, W. Ran, W. Zhang, W. Dai, H. Wang, C. F. Anderson, Z. Wang, C. Zheng, P. Zhang, Y. Li and H. Cui, The Role of Critical Micellization Concentration in Efficacy and Toxicity of Supramolecular Polymers, *Proc. Natl. Acad. Sci. U. S. A.*, 2020, **117**(9), 4518–4526.

36 A. G. Cheetham, P. Zhang, Y. Lin, L. L. Lock and H. Cui, Supramolecular Nanostructures Formed by Anticancer Drug Assembly, *J. Am. Chem. Soc.*, 2013, **135**(8), 2907–2910.

37 H. Su, P. Zhang, A. G. Cheetham, J. M. Koo, R. Lin, A. Masood, P. Schiapparelli, A. Quiñones-Hinojosa and H. Cui, Supramolecular Crafting of Self-Assembling Camp-tothecin Prodrugs with Enhanced Efficacy against Primary Cancer Cells, *Theranostics*, 2016, **6**(7), 1065–1074.

38 A. G. Cheetham, P. Zhang, Y. Lin, L. L. Lock and H. Cui, Supramolecular Nanostructures Formed by Anticancer Drug Assembly, *J. Am. Chem. Soc.*, 2013, **135**(8), 2907–2910.

39 X. He, W. Lu, X. Jiang, J. Cai, X. Zhang and J. Ding, Synthesis and Biological Evaluation of Bis and Monocarbonate Pro-drugs of 10-Hydroxycamptothecins, *Bioorg. Med. Chem.*, 2004, **12**(15), 4003–4008.

40 T. Volk, E. Jähde, H. P. Fortmeyer, K.-H. Glüsenkamp and M. F. Rajewsky, pH in Human Tumour Xenografts: Effect of Intravenous Administration of Glucose, *Br. J. Cancer*, 1993, **68**(3), 492–500.

41 T. Schluep, J. Cheng, K. T. Khin and M. E. Davis, Pharma-cokinetics and Biodistribution of the Camptothecin–Poly-mer Conjugate IT-101 in Rats and Tumor-Bearing Mice, *Cancer Chemother. Pharmacol.*, 2006, **57**(5), 654–662.

This journal is © The Royal Society of Chemistry 2024